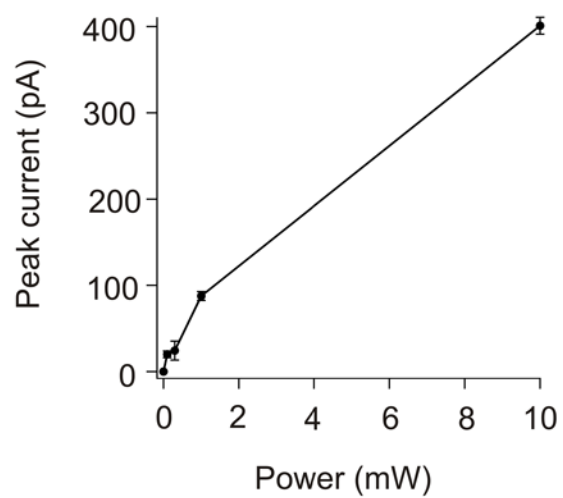
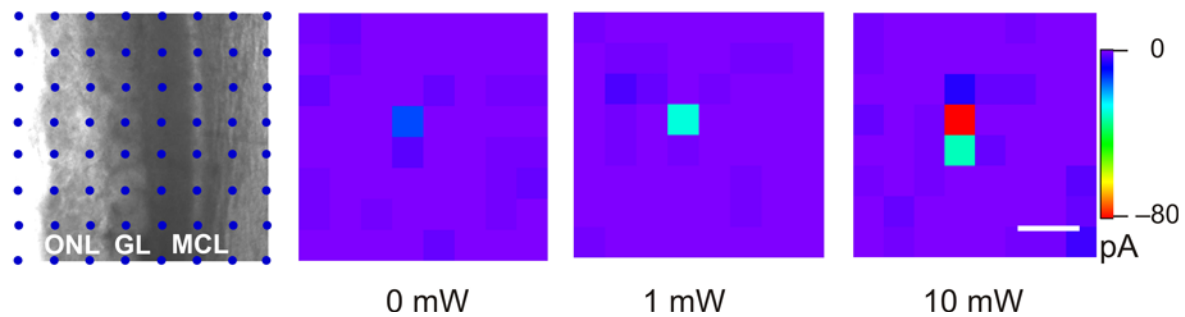


# Fig S1

**a**

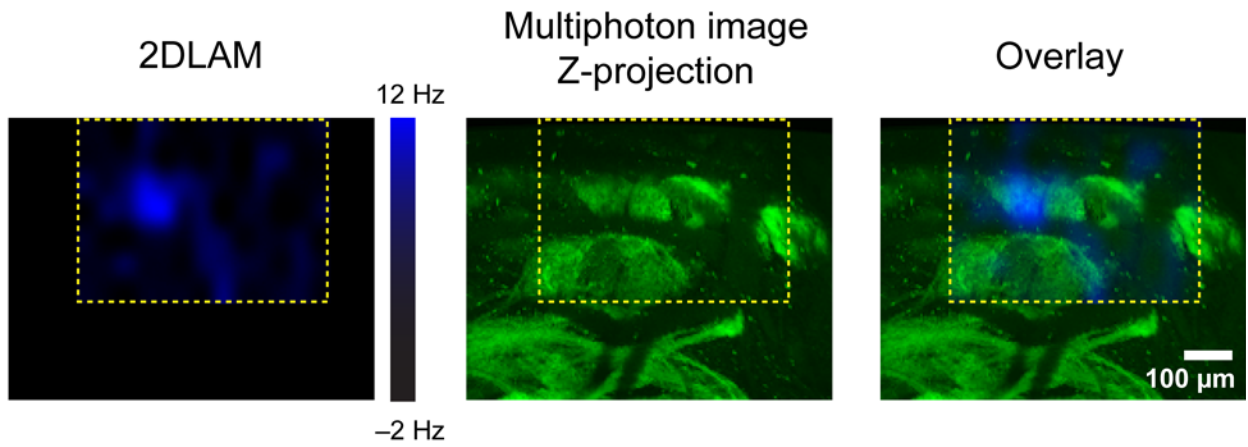


**b**



# Fig S2

**a**



**b**

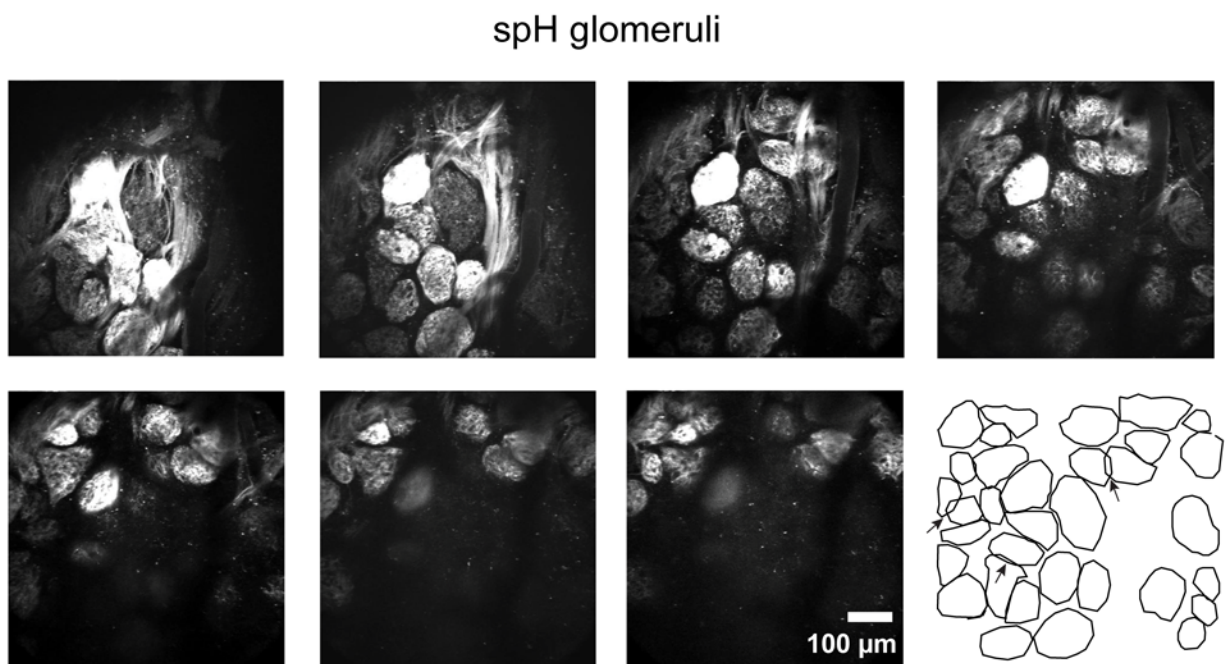


**Fig S3**

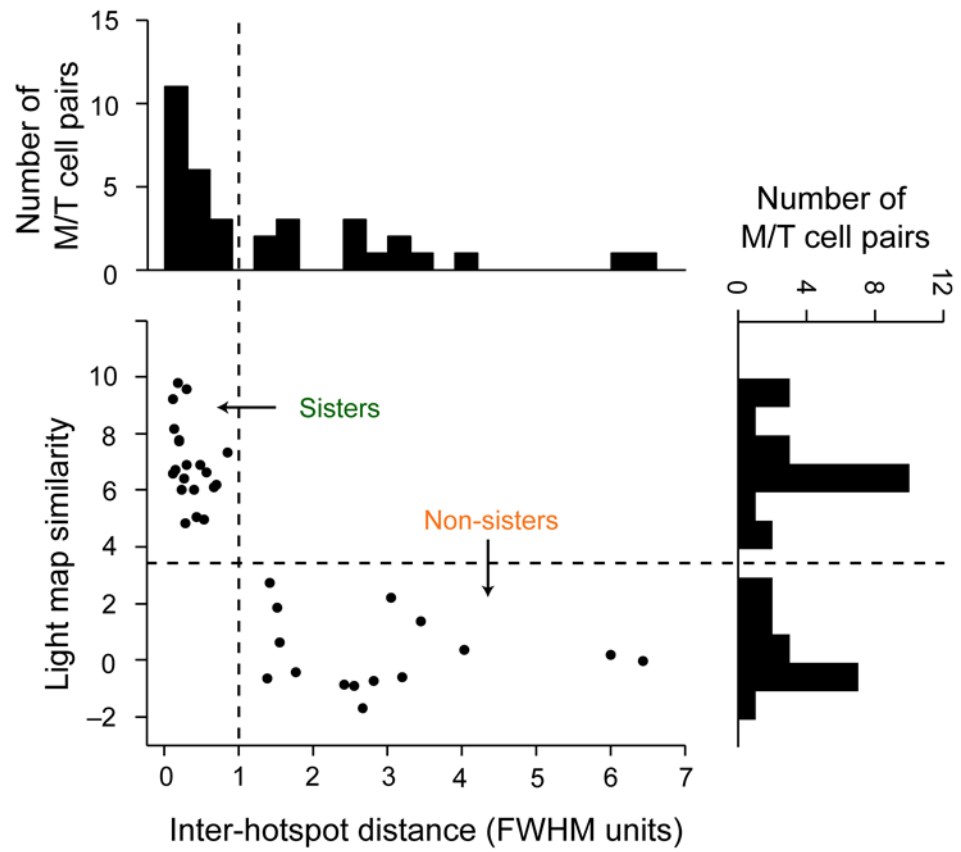


**Fig S4**

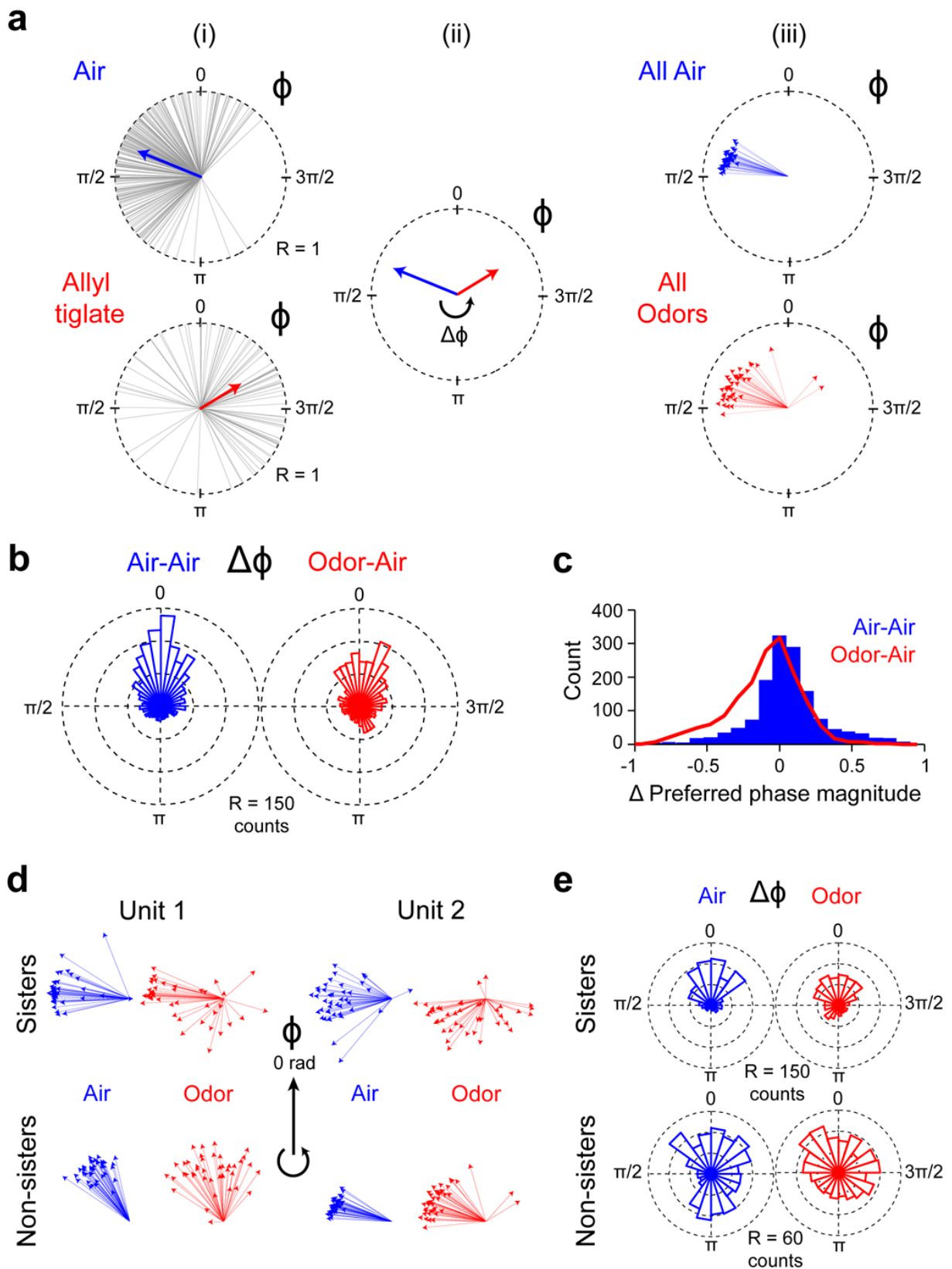


**Fig S5**

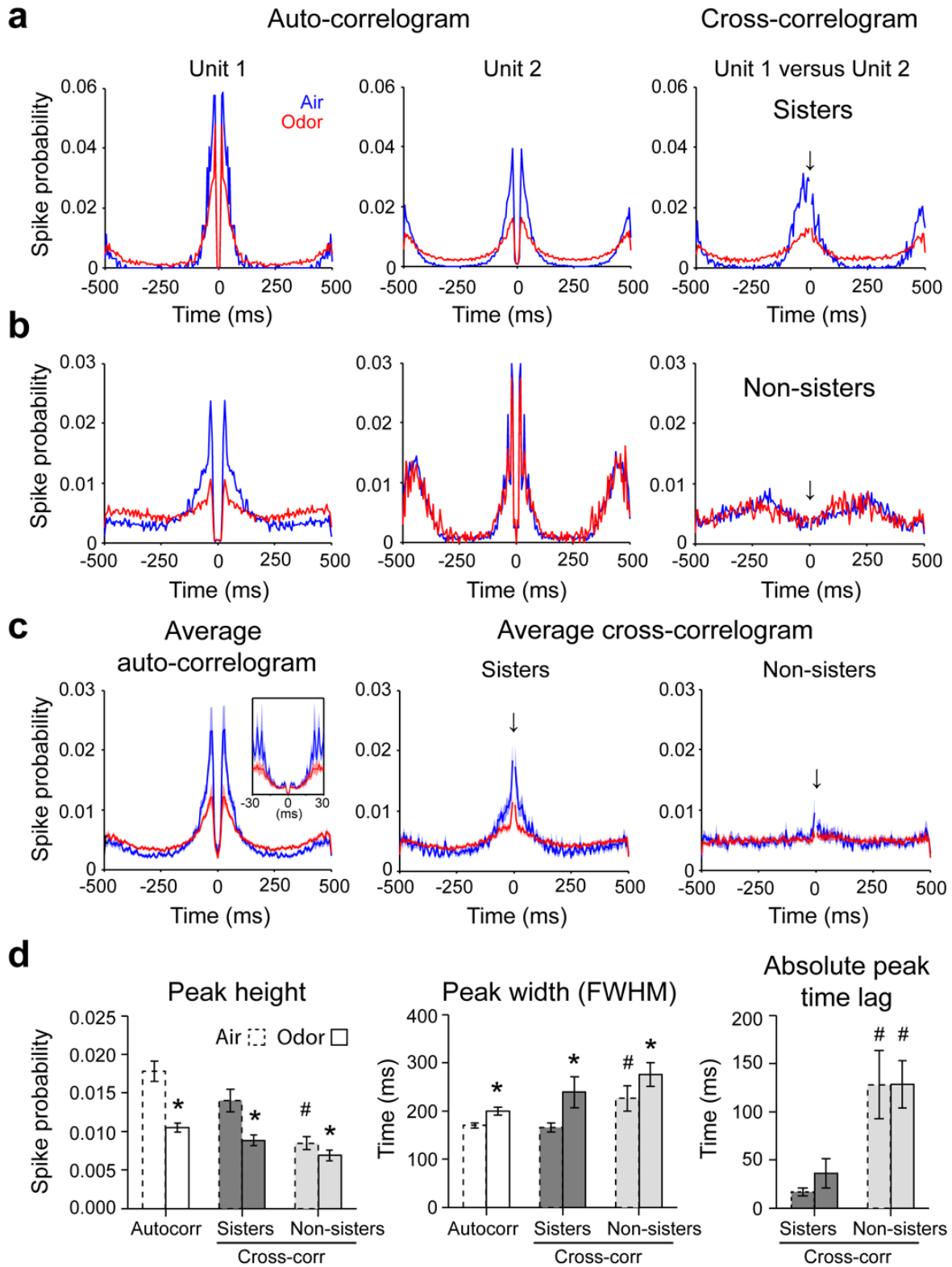
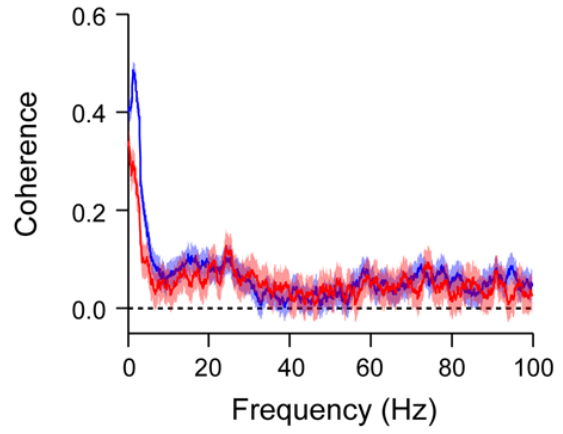
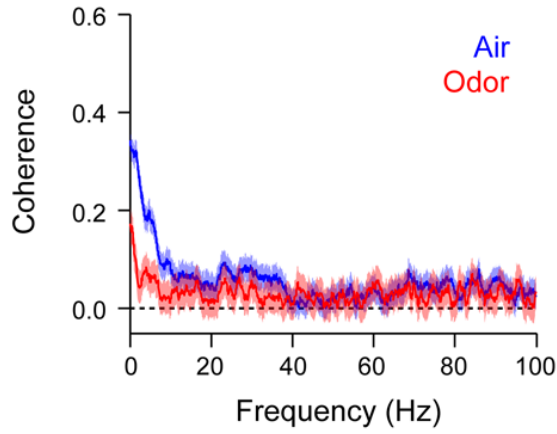
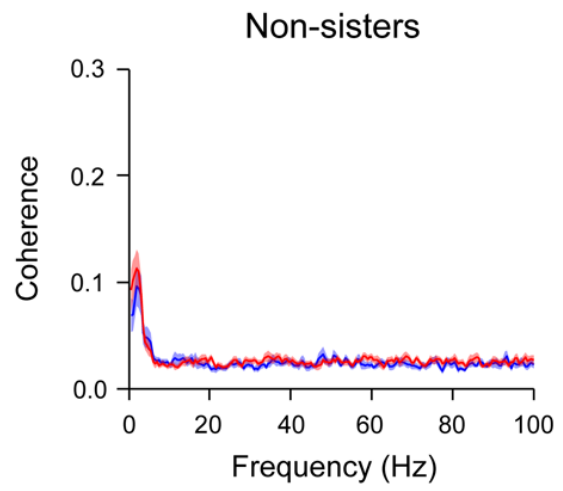
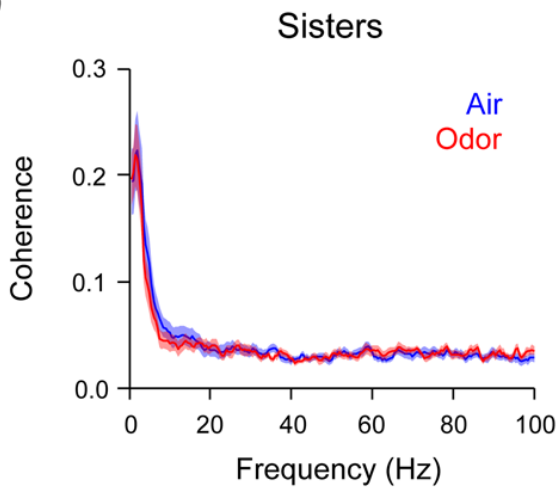


**Fig S6**

**a**



**b**



**c**

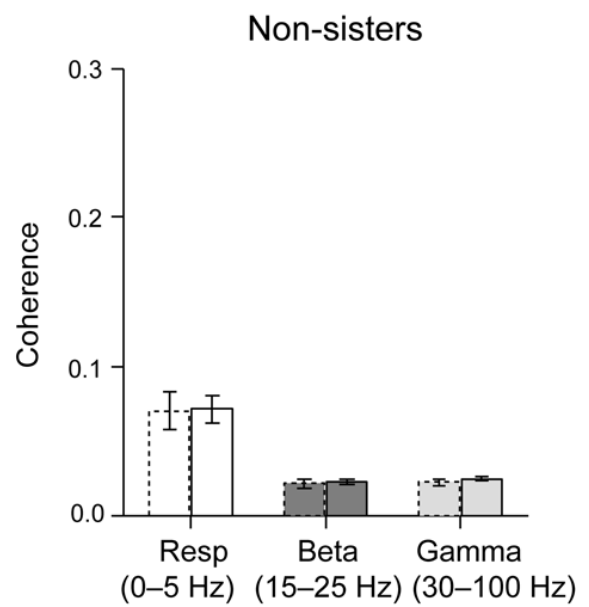
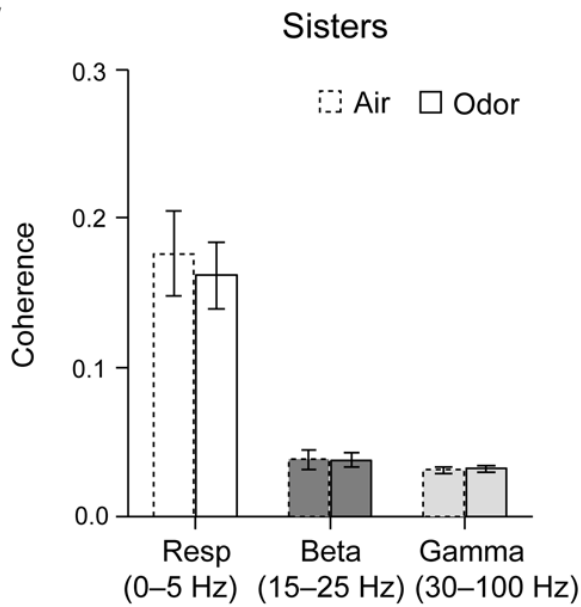
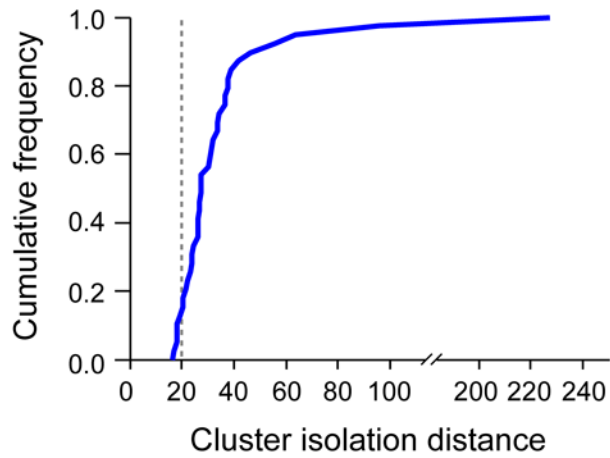
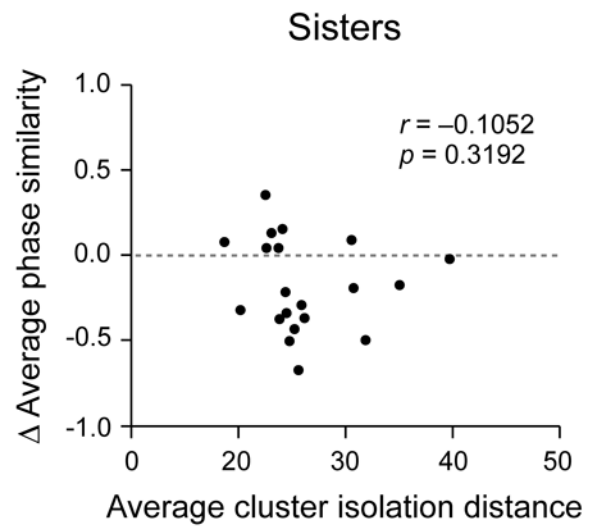


**Fig S7**

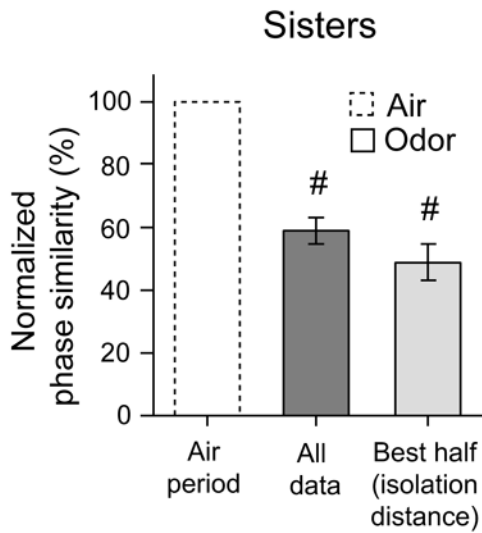
**a**



**b**



**c**



**d**

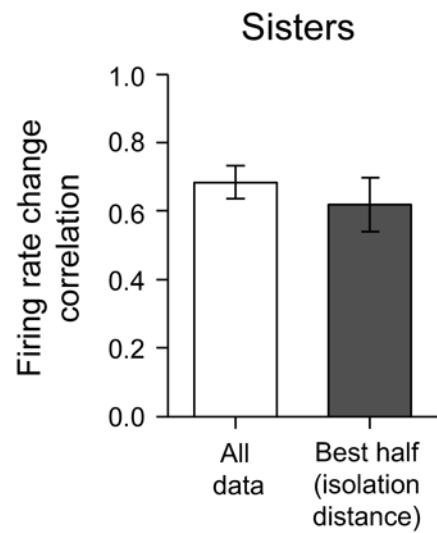
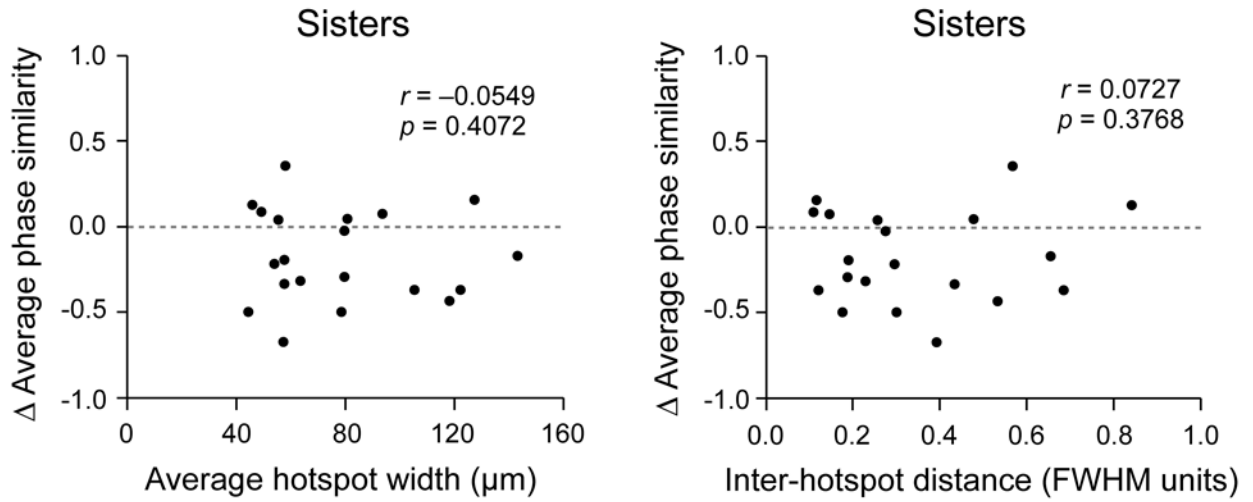
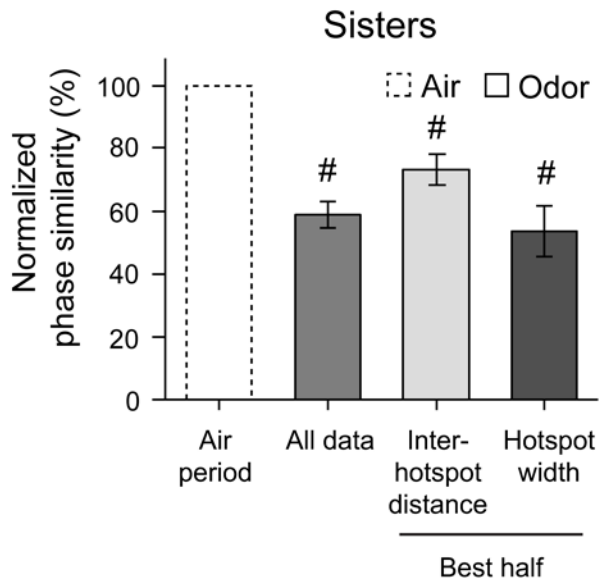


**Fig S8**

**a**



**b**



**c**

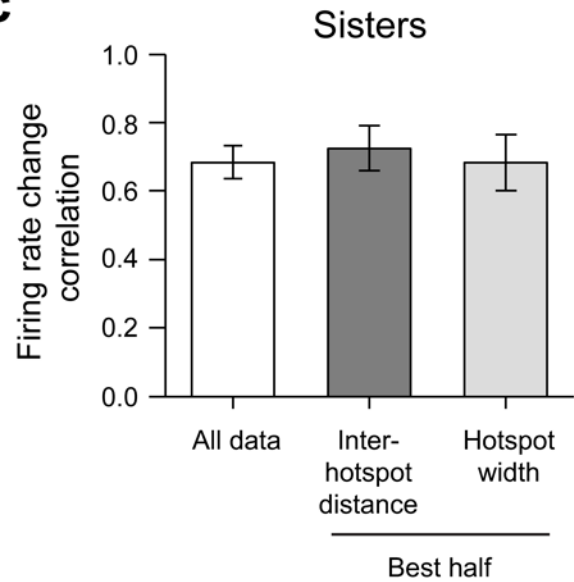
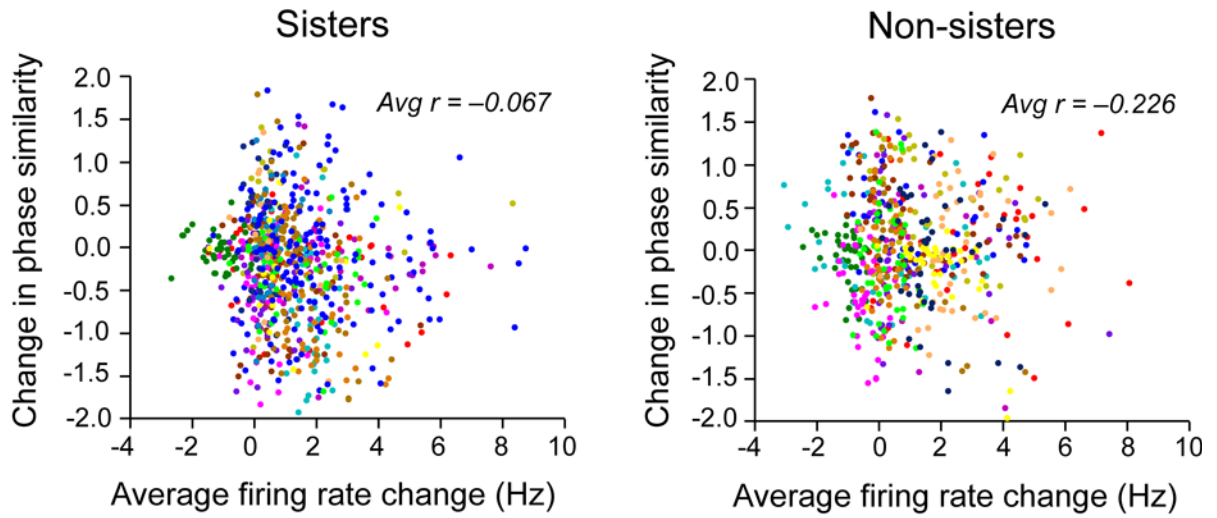
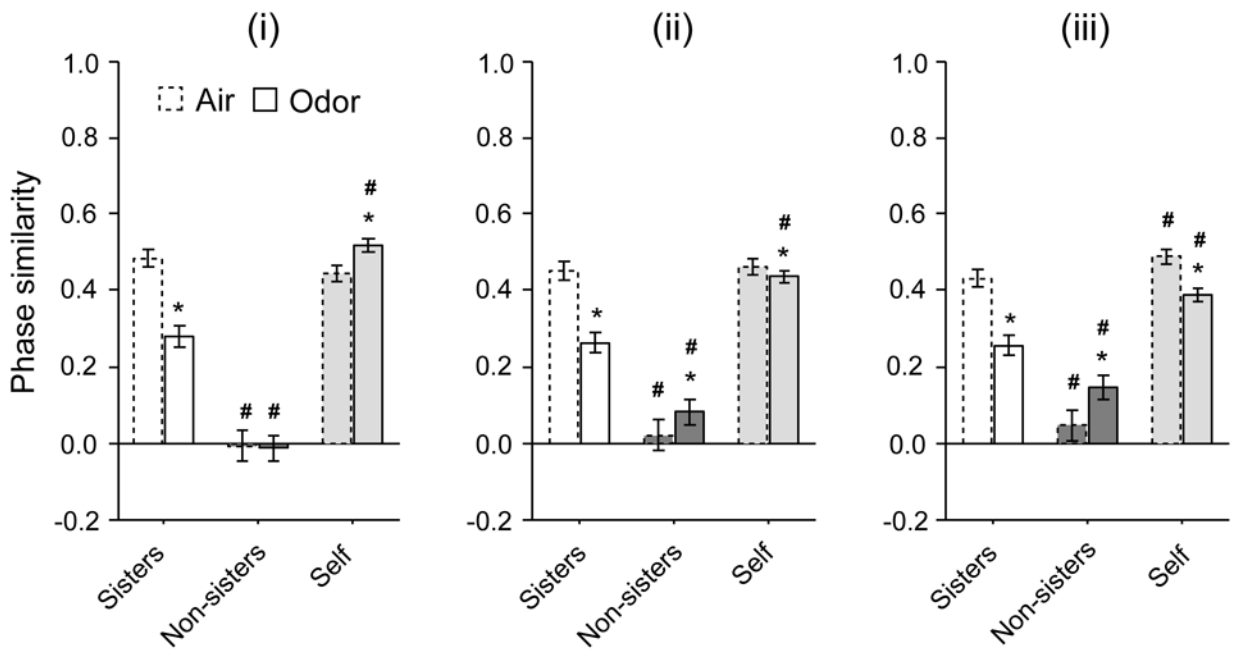


**Fig S9**

**a**



**b**



## Supplementary Information

# Non-redundant odor coding by sister mitral cells revealed by light addressable glomeruli in the mouse

Ashesh K. Dhawale<sup>1,2</sup>, Akari Hagiwara<sup>3</sup>, Upinder S. Bhalla<sup>2</sup>, Venkatesh N. Murthy<sup>3\*</sup> and  
Dinu F. Albeanu<sup>1\*</sup>

1. Cold Spring Harbor Laboratory, One Bungtown Road, Cold Spring Harbor, NY, 11724.

2. National Centre for Biological Sciences, Tata Institute of Fundamental Research, Bellary Road, Bangalore, 560065, India.

3. Dept. of Molecular and Cellular Biology, and Center for Brain Science, Harvard University, 16 Divinity Ave, Cambridge, MA 02138.

### Correspondence:

\*Dinu F. Albeanu                      email: [albeanu@cshl.edu](mailto:albeanu@cshl.edu), tel: 516-367-8822

\*Venkatesh N. Murthy                email: [ynmurthy@fas.harvard.edu](mailto:ynmurthy@fas.harvard.edu), tel: 617-496-4883

## Supplementary Note 1

### Identifying sister and non-sister M/T cells

Using tetrodes, we recorded simultaneously from multiple M/T cells. We used light mapping to determine the parent glomerulus for each recorded M/T cell. A first round of light grid mapping was conducted over the entire exposed bulb surface at a coarse resolution of 150 $\mu$ m and at the highest light intensity of 90 mW/mm<sup>2</sup>, in order to screen the recording site for light responsive units. Each spot in the grid was stimulated for 200 ms in 500 ms long trials. The spots were illuminated in a pseudo-random order for 5 repetitions, and a corresponding two-dimensional light activity map (2DLAM) was generated online for each unit. If more than one light responsive unit was identified, fine-scale light mapping at 75  $\mu$ m or 20  $\mu$ m (sub-glomerular resolution) was then carried out for 10–25 repetitions, over a smaller area of 500–800  $\mu$ m diameter around the recording site. If there were less than two light responsive units, the site was rejected and the electrode was re-inserted into the bulb at a different location. Fine-scale grid maps were generated at successively lower light intensities until no light triggered activity was seen in any unit being recorded. The lowest intensity we used was 2 mW/mm<sup>2</sup>.

Out of 89 mice, only 32 were used for odor experiments, after preliminary online clustering and analysis identified the parent glomeruli of at least one pair of M/T units. Out of the 32 mice used for odor experiments, 15 yielded recording sites that matched all the offline analysis criteria used for single unit identification, and had more than one single unit activated by light per recording site during fine-scale mapping. We focused on

the M/T units that demonstrated light induced activity during fine scale mapping (40 out of 133 units).

We classified pairs of M/T cells into sisters and non-sisters by two different criteria (physical separation of light hotspots and noise corrected correlations of the 2D light activity maps, see **Supplementary Fig. 3**) that produced the same outcome. Some caveats in this classification need to be pointed out.

We defined M/T sister cells as those that project their primary dendrites to the same glomerulus and equated this to them receiving common input from a single type of OSNs. However, there is evidence that a small fraction of glomeruli may be heterogeneous (Albeanu et al., in preparation). Furthermore, anatomical and functional imaging studies (Albeanu et al., in preparation) indicate that glomeruli can be duplicated locally, that is OSNs of a given type may project to close-by glomeruli. Therefore, those cells classified as non-sisters may receive input from the same type of OSNs.

Alternatively, these strong correlations may simply be due to incomplete separation of odor response spectra due to the limited panel of odorants used (that is, due to spurious correlations induced by overlap of glomerular odor responses).

For these reasons, our population of sister and non-sister units may have slight contamination in both directions. However, since biases arising from the caveats listed above would only diminish the underlying contrast between sister and non-sister pairs, the actual differences in functional properties between the two classes are likely to be even greater than the observed differences (which are already highly significant).

A higher than expected ratio of sister to non-sister M/T pairs (20 versus 15), is due to the following reasons. First, we pre-selected recording sites that had mainly sister pairs for odor stimulation, as indicated by preliminary online clustering during light mapping. This was done to overcome the intrinsically low chance (20–30%) of recording sister pairs\*. Second, ChR2-YFP expression in the ORC mice used in this study was heterogeneous (**Fig. 1a** and **Fig. 3d**, see Methods), similar to the OMP-spH mouse<sup>10</sup> (**Supplementary Fig. 2b**). Thus not all glomeruli were equally excitable by light. When considering the range of possible M/T unit combinations, this bias intrinsically leads to an increase in the relative proportion of sister versus non-sister pairs.

A potential complication that one must control for when using the ORC mice is contamination resulting from activation of fibers of passage versus glomeruli *per se*. We observed hotspots that were non-spherical (streaks, for example) only at high light intensities. We interpret these to be bundles of homotypic axons converging on the parent glomerulus of the recorded M/T cell. As light intensity was lowered, only the prominent spherical hotspot remained in place. Since the highest density of homotypic axons occurs within the glomerulus, the lowest threshold of M/T response should also be in the glomerulus. We sought to minimize nonspecific activation of OSN fibers, by iteratively adjusting the size and intensity of light spots in order to operate in a minimal stimulation regime.

## Supplementary Note 2

### Odors trigger distinct changes in the average phase preference of sister M/T cells

To characterize the timing of discharge of individual M/T units under different conditions, we calculated two parameters: the preferred phase of firing ( $\phi$ ) relative to respiration and the magnitude of this phase preference (M) for any given stimulus (**Supplementary Fig. 4a i**; each gray radial line marks the occurrence of a spike at a particular phase in the cycle). For each unit, these measures were calculated during Air and Odor, and displayed in vector form (**Supplementary Fig. 4a**). We then calculated the odor induced changes (Odor-Air) in the average phase angles ( $\Delta\phi$ ) and preferred phase magnitude ( $\Delta M$ ), and compared these to the fluctuations in  $\phi$  and M during Air alone (Air-Air), across trials. On average, odors caused significant differences in phase angle, as well as a decrease in the magnitude of phase preference (**Supplementary Fig. 4b–c**,  $p = 0.003$  and  $p < 10^{-5}$ , two-sample Kuiper test and paired t test respectively).

What is the relationship between the phase preferences of simultaneously recorded units? In the example shown in **Supplementary Fig. 4d**, during Air, the sister pair (top) had overlapping phase vectors (pointing towards  $\pi/2$ ), whereas the non-sister pair preferred different phases (bottom). All four units showed a broader range of phase angles and shorter vector lengths during Odor, indicating phase dispersion as well as a reduction in the magnitude of phase-locking with respiration.

The distribution of inter-unit phase differences is shown as circular histograms in **Supplementary Fig. 4e** for both sister and non-sister pairs during Air and Odor. For M/T pairs, phase differences were largely distributed around zero radians during Air, and,

upon odor presentation, the distribution broadened (**Supplementary Fig. 4e**, *Top*, two-sample Kuiper test,  $p = 0.001$ ). For non-sister pairs, the phase differences had multiple preferred locations (for example, close to 0 and  $\pi$ ) during Air, and were dispersed further upon odor stimulation (**Supplementary Fig. 4e**, *Bottom*, two-sample Kuiper test,  $p = 0.001$ ).

### Supplementary Note 3

#### Odors induce broadening of spike time correlations of M/T cell pairs

To examine more directly the spiking relationship between pairs of M/T units, we turned to the commonly used spike time correlation analysis. For both Air and Odor conditions, we calculated auto-correlograms for individual M/T units and, correspondingly, cross-correlograms for M/T cell pairs (**Supplementary Fig. 5a–c**).

All auto-correlograms had a valley at 0 ms corresponding to the refractory period of the neuron. The valley was nested in the zero order peak of the auto-correlogram, with secondary peaks at time intervals corresponding to respiratory cycle duration (**Supplementary Fig. 5a–c**). Closer inspection also revealed periodic modulation of spikes in the gamma frequency range, as described before<sup>16</sup> (**Supplementary Fig. 6**), but we chose to focus here on the respiration locked modulation. Representative and average cross-correlograms of spikes from sister pairs indicated synchronous firing over time scales of ~150 ms (**Supplementary Fig. 5a,c**, right and center panel respectively). Different non-sister pairs had delays spread throughout the duration of the respiratory cycle, such that the peaks canceled out when pooled across all non-sister cross-correlograms (**Supplementary Fig. 5b,c**, right panels).

We smoothed all correlograms to extract several parameters that describe odor induced changes in the temporal dynamics of recorded units (see Supplementary Methods): peak height, width (FWHM) and absolute shift of the peak with respect to zero time. On average, odor presentation caused significant broadening of the peak and a drop in peak height of the M/T units' auto-correlograms, as well as of both sister and non-sister pairs'

cross-correlograms (**Supplementary Fig. 5a,c**, but see **5b**, center panel, **5d**, left and center panels,  $p < 0.05$ , two-sample paired t test). In addition, odors did not induce any significant shift in the peak position of the cross-correlogram for sister and non-sister pairs (**Supplementary Fig. 5d**, right panel,  $p = 0.42$  and  $0.43$ , two-sample paired t test).

Interestingly, odor presentation brought the average peak height and average FWHM of sister M/T pairs to values similar to those of non-sister M/T pairs during Air ( $p = 0.74$ , and  $p = 0.79$ , two-sample unpaired t test). As expected, within the Air condition, the non-sister M/T pairs had consistently lower peaks, wider FWHMs, and longer absolute time shifts in cross-correlograms compared to sister pairs ( $p < 0.05$ , two-sample unpaired t test, **Supplementary Fig. 5d**). However, during Odor, the peak height and FWHMs were not distinguishable for sister and non-sister pairs ( $p = 0.07$  and  $p = 0.44$ ).

## Supplementary Note 4

### Spike train coherence

We calculated the spike train coherence during Air and Odor conditions pooling all stimuli, using Chronux analysis toolbox (<http://chronux.org>) and multi-taper methods.

We note that most of the power in the coherence spectrum lies in the respiratory frequency range (0–5Hz). We did observe peaks at higher frequencies, namely in the beta and gamma bands (15–25 Hz and 30–100 Hz respectively), as shown in **Supplementary Fig. 6a**. However, on average, we did not find significant power in these bands.

We note that odors did not trigger significant alteration in coherence within the respiration band. Given our reports of odor induced changes of cross-correlogram shape at the respiratory time scale, this result may appear counterintuitive. However, it can be readily explained by taking into account that odors produced changes in the shapes of both auto and cross-correlograms to similar degrees. Since coherence is the cross-spectral density normalized by the product of the auto-spectral densities of the two units, it need not change.

## Supplementary Note 5

### Quality controls of criteria for unit isolation and sister-pair separation

The odor-induced drop in phase similarity observed between sister units did not correlate with either the quality of unit isolation, as measured by the isolation distance<sup>48</sup> of individual unit clusters, nor the width of their hotspots or the distance between them (**Supplementary Figs. 7b and 8a**). Furthermore, on the basis of the above criteria, selecting the best 10 sister pairs (in terms of the highest isolation distance, smallest hotspot FWHM, or shortest inter-hotspot distance), produced the same results as the entire population of sister pairs (**Supplementary Figs. 7c, d and 8b, c**).

## Supplementary Note 6

### Odor induced phase and firing rate changes are independent

In much of our study, we separately probed either odor induced alteration in average firing patterns (firing rate changes) or temporal dynamics of M/T cell responses (phase correlations). In several examples, we found that sister M/T units behaved differently when considering firing rate versus phase correlation modulations, therefore we wanted to understand whether there is any systematic relationship between the two.

We first compared odor induced changes in firing rates with changes in the phase similarity for each M/T pair across all stimuli (**Supplementary Fig. 9a**). The relation between the modulation of phase similarity against the mean firing rate change for pairs of units showed a wide spread of values, with minimal correlation trend. For example, for sister units, the average correlation between changes in firing rate and phase similarity modulation was as low as  $-0.067$  ( $p = 0.14$ , in comparison to shuffled control, paired t test), and for non-sister M/T pairs was  $-0.226$  ( $p = 0.004$ ).

We further wondered whether the phase dispersion between pairs of units depends on a subset of odors that elicit strong firing responses. Therefore, we decided to split the 42 stimuli into three groups based on their absolute firing rate changes and measure the phase similarity for each group (**Supplementary Fig. 9b**). One unit of each pair was selected pseudo-randomly to be the seed for ranking odors. The trends seen in the whole set of odors (**Fig. 7e, f**) were consistently present in all three subsets (**Supplementary Fig. 9b**).

- \* Schoppa, N.E. & Westbrook, G.L. Glomerulus-Specific Synchronization of Mitral Cells in the Olfactory Bulb. *Neuron* **31**, 639-651(2001).

## Supplementary figure legends

### Supplementary Figure 1: Effects of changing laser intensity on light induced M/T current responses in olfactory bulb slices from ORC mice

**a.** Effects of varying laser intensity on synaptic currents in the same mitral cell as shown in **Fig. 1c**. LSPS was performed at each point in an 8X8 grid covering the ONL, GL, EPL and MCL of the olfactory bulb slice. (*Left*) The grid is shown overlaid on top of the slice; (*Right*) Three 2DLAMs obtained at different photo-stimulation laser powers.

**b.** Average peak synaptic currents elicited in the recorded mitral cell across five photo-stimulation laser power levels and four repeats.

### Supplementary Figure 2: Matching functional hotspots to anatomical glomeruli

**a.** (*Left*) Functional hotspot from representative two dimensional light activated map (2DLAM); (*Center*) Z-stack image projection of anatomical glomeruli from the same field of view as the 2DLAM obtained via multiphoton microscopy. (*Right*) Overlay of the 2DLAM and the z-projection. Yellow dotted lines indicate the boundaries of the 2DLAM.

**b.** Example z-stack image projections of OMP-spH glomeruli obtained via multiphoton microscopy. Each optical section is a 20  $\mu\text{m}$  thick projection, taken 20  $\mu\text{m}$  apart in the z-axis from the subsequent one. Drawing illustrates contours of the glomeruli in the field of view. Arrows indicate overstacked glomeruli.

**Supplementary Figure 3: Classification of M/T cells into sisters and non-sisters using two criteria**

(Top) Separation of M/T cells into sisters and non-sisters based on Euclidean distance between the centers of light hotspots on 2DLAMs, as shown in **Fig. 3f**; (Right)

Distribution of mean pair-wise correlations ( $N = 35$ ) of the measured 2DLAMs relative to the mean correlations of scrambled 2DLAMs (right marginal distribution). Light map similarity refers to how far away from chance the measured correlation coefficients between 2DLAMs of all considered pairs are. The chance distribution of correlation coefficients was obtained from scrambling 2DLAMs 1,000 times. The similarity distance is expressed in units of standard deviations of scrambled 2DLAMs' noise correlation distribution. Zero corresponds to the mean of the scrambled 2DLAMs distribution. The dotted lines demarcate non-sister M/T cells (Right, Bottom) from sister cells (Left, Top) and are placed at 1 FWHM, and 3.5 standard deviations distance from the mean correlation of the scrambled 2DLAMs, respectively.

**Supplementary Figure 4: Odors induce dissimilar changes in average phase vectors for sister and non-sister M/T pairs**

**a.** (i) Schematic illustrating the calculation of average phase vectors during Air (*top*) and Odor (*bottom*) for one stimulus (allyl tiglate). Phase angles were assigned ranging from 0 to  $2\pi$  radians to all spikes of M/T units based on their occurrence time within the respiratory cycle, where 0 radians referred to the start of inspiration. Each spike could then be defined as a unit vector. The average phase vector was computed by taking the vector sum of all such spike vectors within a defined condition (Air or Odor periods) and normalizing its length by the number of spikes. The angle of the average phase vector ( $\phi$ ) denoted the mean phase of spiking, while its length, ranging from 0 to 1, indicated the degree of phase preference, with 1 indicating that all spikes occurred at the same phase. (ii) The average phase vectors for Air (blue) and Odor (red) for this stimulus are shown on the same polar plot to illustrate the change in phase ( $\Delta\phi$ ) and vector length ( $\Delta M$ ) between Air and Odor periods. (iii) The average phase vectors are shown for all Air (*Top*, blue) and Odor (*Bottom*, red) periods for one M/T unit;  $\phi$  - average phase vector angle,  $R$  - unit angle vector length.

**b.** Circular histograms of differences in average phase angles between Air period split across trials (*Left*) and between Odor and Air periods (*Right*) for each recorded M/T unit ( $N = 42$  stimuli X 40 units). Dashed concentric circles indicate intervals of 50 pair-wise comparisons;  $R$  is the radius of the plot in numbers of pair-wise comparisons (counts).

**c.** Distribution of pair-wise differences in preferred phase magnitude (the length of the phase vector in panel **A** for each unit between Air and Odor; Air-Air distribution (blue) refers to comparison between two different blocks of trials during the Air period; Odor-Air refers to comparison between Odor and Air for each unit ( $N = 42$  stimuli X 40 units).

**d.** Average phase vectors plotted for 42 fresh air (blue) and odor (red) stimuli for example units (Unit 1 and Unit 2) of sister (*Top*) and non-sister (*Bottom*) M/T pairs. The length of the vertical arrow indicates phase preference magnitude ( $M$ ) of 1, and orientation defines  $\phi = 0$  radians or the start of the respiratory cycle; phase increases counter-clock wise.

**e.** Circular histograms of inter-unit differences in average phase angles ( $\Delta\phi$ ) between sister ( $N = 20$ ) (*Top*) and non-sister ( $N = 15$ ) (*Bottom*) pairs, for Air (*Left*, red) and Odor (*Right*, blue) conditions across 42 stimuli. Dashed concentric circles indicate intervals of 50 and 20 pair-wise comparisons between sisters and non-sisters respectively.

Differences in the average phase angles were computed in the order: phase leading cell – phase lagging cell. For each M/T pair, the phase leading cell was defined as the cell which, on average, had phase angles closer to the start of inspiration (phase = 0 degrees) during odor periods. The other unit of the pair was termed the phase lagging cell.

**Supplementary Figure 5: Odors induce broadening of spike-time auto and cross-correlograms for sister and non-sister M/T units**

**a.** (*Left, Center*) Example spike-time auto-correlograms for two sister M/T units (1 and 2), generated over all stimuli for Air (blue) and Odor (red) periods; (*Right*) Example cross-correlogram between these units (1 and 2) generated over all stimulus presentations during Air (red) and Odor (blue) periods. The bin width for all correlograms was 5 ms, and they are normalized to the total number of spikes.

**b.** (*Left, Center*) Example spike-time auto-correlograms for two non-sister M/T units (1 and 2), generated over all stimuli for Air (blue) and Odor (red) periods; (*Right*) Example cross-correlogram between these units (1 and 2) generated over all stimulus presentations during Air (red) and Odor (blue) periods.

**c.** (*Left*) Average auto-correlogram and cross-correlogram calculated for all sister (*center*) and non-sister (*right*) M/T cell pairs. (*Left Inset*) A closer look at the average auto-correlogram at 1ms bin time resolution. Center bins of the cross-correlograms (0 ms) were not calculated because simultaneous spikes were not detected (arrows).

**d.** Normalized correlograms were smoothed by fitting cubic splines (function ‘csaps’ in MATLAB; smoothing parameter =  $10^{-5}$ ), followed by extraction of the following parameters: peak amplitude, peak width and peak time lag (from 0 ms). (*Left*) Peak heights of auto-correlograms for all M/T cells ( $N = 38$ ) and of cross-correlograms for all sister ( $N = 16$ ) and non-sister M/T pairs ( $N = 9$ ); Air (dotted line) and Odor (continuous line) intervals. (*Center*) Peak width measured as full width at half max (FWHM) for auto-correlograms for all M/T unit cells and for cross-correlograms for sister and non-sister M/T pairs. (*Right*) Absolute peak time lag (with respect to 0 ms) in cross-correlograms for sister and non-sister M/T pairs; \* marks  $p < 0.05$  for the same group of units (sister or non-sister M/T units) across conditions (Odor vs. Air); # marks  $p < 0.05$  for the same condition (Air or Odor), across groups (e.g. sister versus non-sister M/T pairs).

The central valley ( $\pm 30$  ms) in the auto-correlograms was not used for the cubic spline fitting; instead peak parameters were extrapolated from the fit. These parameters were

only calculated for those correlograms that had a significant peak height, defined as twice the standard deviation of the noise in the correlogram.

### **Supplementary Figure 6: Spike train coherence between M/T pairs**

- a.** Example coherence spectra of two sister M/T pairs during Air (blue) and Odor (red) periods; confidence intervals are indicated by dotted lines,  $p < 0.05$ .
- b.** Average coherence spectrum for sister (*Left*) and non-sister (*Right*) M/T pairs.
- c.** Average coherence across different frequency bands (respiration range 0–5Hz, beta 15–25Hz, gamma 30–100Hz) for sister (*Left*) and non-sister (*Right*) M/T pairs.

### **Supplementary Figure 7: Relationship between cluster Isolation Distance and response properties of sister M/T pairs**

- a.** Cumulative distribution of Isolation Distance values for all single unit clusters (Median = 27.1,  $N = 40$ ).
- b.** Distribution of average drop in phase similarity between Air and Odor conditions, across all stimuli, for sister M/T pairs plotted against corresponding average cluster Isolation Distance values.
- c.** Average phase similarity, normalized with respect to Air (*left*) for Odor condition, across all stimuli for all sister pairs (*center*) and best half of sister pairs ranked in terms of average cluster isolation distance values (*right*).

**d.** Average firing rate change correlation for all sister pairs (*left*) and best half of sister pairs ranked in terms of average cluster isolation distance values (*right*).

**Supplementary Figure 8: Relationship between firing and phase properties of sister M/T pairs, and hotspot width or inter-hotspot distances**

**a.** (*Left*) Average drop in phase similarity between Air and Odor conditions, across all stimuli, for sister M/T pairs plotted against corresponding average hotspot width (FWHM) values. (*Right*) Average drop in phase similarity between Air and Odor conditions, across all stimuli, for sister M/T pairs plotted against corresponding average inter-hotspot distance (in FWHM units).

**b.** Average phase similarity, normalized with respect to Air (*dotted line*) for Odor condition (continuous line), across all stimuli for all sister pairs and best half of sister pairs ranked in terms of shortest inter-hotspot distance and smallest hotspot width (FWHM) respectively.

**c.** Average firing rate change correlation for all sister pairs and best half of sister pairs ranked in terms of shortest inter-hotspot distance and smallest hotspot width (FWHM) respectively.

**Supplementary Figure 9: Phase versus firing rate changes in sister and non-sister M/T cell pairs**

- a.** Change in inter-unit phase similarity between Odor and Air plotted against corresponding average changes in firing rate for sister (*Left*) and non-sister (*Right*) M/T unit pairs. Different colors correspond to different pairs.
- b.** Phase similarities for three groups of odors ranked by their strength in terms of absolute firing rate changes (i –strong, ii – medium, iii – weak) calculated during Air (dotted lines) and Odor (continuous lines) conditions; \* marks  $p < 0.05$  for same group of units (sister or non-sister M/T units) across conditions (Odor vs. Air); # marks  $p < 0.05$  for same condition (Air or Odor), across groups (e.g. sister versus non-sister M/T units).

Supplementary Table 1: List of odors used in experiments

Odor Number	Odor Name	Concentration (% of Saturated Vapor Pressure)
0	peppermint oil	
1	propyl tiglate	
2	valeraldehyde	
3	2-methoxypyrazine	2.07 ± 0.150
4	cyclohexyl ethyl acetate	
5	p-anis aldehyde	
6	ethyl valerate	0.38 ± 0.027
7	propyl butyrate	0.70 ± 0.041
8	ethyl heptanoate	
9	allyl tiglate	0.51 ± 0.014
10	isoamylamine	1.14 ± 0.093
11	valeric acid	
12	methyl tiglate	1.26 ± 0.057
13	hexanoic acid	
14	gamma terpinene	1.00 ± 0.015
15	heptanal	0.70 ± 0.025
16	isoamylacetate	0.44 ± 0.036
17	hexanal	0.25 ± 0.020
18	2-heptanone	1.15 ± 0.065
19	1-pentanol	0.09 ± 0.006
20	air	
21	mineral oil	
22	2,3-pentanedione	
23	ethyl hexanoate	
24	pyrrolidine	
25	allyl butyrate	
26	ethyl tiglate	
27	methyl tiglate	0.46 ± 0.089
28	verbenone	
29	4-heptanone	
30	ethyl propionate	
31	ethyl butyrate	
32	isobutyl amine	
33	2-hexanone	
34	isobutyl propionate	
35	pentyl acetate	
36	butyl propionate	
37	nutmeg oil	
38	methyl butyrate	
39	phenyl ethyl acetate	
40	ethyl acrylate	
41	carvyl acetate	